annalen der physik
www.ann-phys.org

Evaluation of Charged Defect Energy in Two-Dimensional Semiconductors for Nanoelectronics: The WLZ Extrapolation Method

Sha Xia, Dan Wang, Nian-Ke Chen, Dong Han, Xian-Bin Li,* and Hong-Bo Sun*

Defects play a central role in controlling the electronic properties of two-dimensional (2D) materials and realizing the industrialization of 2D electronics. However, the evaluation of charged defects in 2D materials within first-principles calculation is very challenging and has triggered a recent development of the WLZ (Wang, Li, Zhang) extrapolation method. This method lays the foundation of the theoretical evaluation of energies of charged defects in 2D materials within the first-principles framework. Herein, the vital role of defects for advancing 2D electronics is discussed, followed by an introduction of the fundamentals of the WLZ extrapolation method. The ionization energies (IEs) obtained by this method for defects in various 2D semiconductors are then reviewed and summarized. Finally, the unique defect physics in 2D dimensions including the dielectric environment effects, defect ionization process, and carrier transport mechanism captured with the WLZ extrapolation method are presented. As an efficient and reasonable evaluation of charged defects in 2D materials for nanoelectronics and other emerging applications, this work can be of benefit to the community.

1. Introduction

The studies of two-dimensional (2D) materials and their applications started from the work of producing graphene via a mechanical exfoliation by Novoselov et al. in 2004.[1] Recently, the applications of 2D semiconductors go further and faster.[2–7] In 2014, a p–n junction diode based on the electrostatically doped monolayer WSe_2 was demonstrated for solar-energy conversion and light emission.[8] This result indicates that 2D semiconductors have great potential in optoelectronics. More progress of 2D optoelectronics and photonics is introduced in two recent reviews.[9,10] In 2016, Desai et al.[11] fabricated a 1-nm gate-length field effect transistor (FET) with high-electron mobility and switching characteristics using carbon nanotube as gate and MoS_2 as a channel. Therefore, 2D semiconductors are also considered as next-generation channel materials for lower power and higher integrated devices. In addition, 2D semiconductors, such as transitional metal dichalcogenide (TMD), can be used as a dielectric layer for memory due to their stable nonvolatile resistance switching.[12–14] For example, Ge et al.[15] reported an atomristor in TMD monolayers sandwiched between metal electrodes in 2018. In fact, the development of neuromorphic computing and nonvolatile flexible memory could be benefited from the widespread application of 2D semiconductors. More importantly, 2D semiconductors can possibly bring new hope to extend Moore's Law.[16] Generally, due to the decrease of dimension, 2D semiconductors hold many novel and unique physical/chemical properties,[17–21] which make them as competitive candidates to replace traditional semiconductor materials.

However, the industrialization of electronic devices based on 2D semiconductors still has a long way to go. One of the key matters is how to achieve reliable and stable n-/p-type conductivity to realize basic building blocks, such as p–n junction and complementary metal–oxide–semiconductor units.[22] Though defect in materials destroys the structural integrity, it could have a positive impact on controlling its electrical and semiconductor properties.[23] For example, defect causes the change of the band gap, the change in the actual number of carriers, and the change in the mobility, so that the material can exhibit n-type or p-type conductivity.[24–26] Therefore, it is also a good method to employ defects to control conductivity for 2D semiconductors. For example, Cao et al.[27] realized a stable p-type conductivity in 2D WS_2 by incorporating substituted nitrogen (N) atoms in the lattice instead of charge transfer doping.[28] **Figure 1**a shows the nitrogen-doped WS_2 FET fabricated on a 2 in. SiO_2/Si wafer as well as a

S. Xia, Dr. N.-K. Chen, Prof. X.-B. Li, Prof. H.-B. Sun
State Key Laboratory of Integrated Optoelectronics, College of Electronic Science and Engineering
Jilin University
Changchun 130012, China
E-mail: lixianbin@jlu.edu.cn
Dr. D. Wang
Department of Materials Science and Engineering
Rensselaer Polytechnic Institute
Troy New York 12180, USA
E-mail: wangd11@rpi.edu
Dr. D. Han
State Key Laboratory of Luminescence and Applications, Changchun Institute of Optics, Fine Mechanics and Physics
Chinese Academy of Sciences
Changchun 130033 China
Prof. H.-B. Sun
State Key Lab of Precision Measurement Technology and Instruments, Department of Precision Instrument
Tsinghua University
Beijing 100084 China

DOI: 10.1002/andp.201900318

schematic of the atomic model for the doped WS_2. The synthesis process is shown in Figure 1b where a WO_xN_y film is fabricated by atomic layer deposition (ALD) and then a wafer-scale WS_2 film is prepared by a further sulfurization of WO_xN_y film. In Figure 1c, X-ray photoelectron spectroscopy (XPS) spectra demonstrate that nitrogen atoms are successfully doped into the WS_2 films. Additionally, the manufactured WS_2 back-gate FETs exhibit an unambiguous p-type conductivity, as shown in Figure 1d. Another two examples are the p–n heterojunction-based photovoltaic solar cells that were fabricated by intentionally or intrinsically doped 2D semiconductors in Wi et al.[29] (Figure 1e) and Cho et al.'s work[30] (Figure 1f). Moreover, most recently, Momose et al.[31] employed chemical vapor deposition technique to synthesize a p-type MoS_2 by doping phosphorus atom at S site. Figure 1g shows a van der Pauw (vdP) device configuration with the p-type sample, which holds a significantly enhanced conductivity (with ohmic behavior) compared to the undoped MoS_2 as shown in Figure 1h.

To date, free carriers in semiconductors for most electronic devices are supplied by intrinsic or extrinsic defects,[22,25] necessitating a sufficient understanding of defects. A theoretical property prediction is crucial before utilizing charged defect for technological implementations, as it is not practical, or at least not economical, to experimentally curate and investigate every kind of defect to identify the most desirable one. Usually, the concentration of carriers ionized by one defect is evaluated by calculating the formation energy and ionization energy (IE).[22] Within the first-principles calculations framework, the periodic boundary condition is invoked, resulting in long-range coulomb interaction between a charged defect and its images, and consequently an energy divergence. A homogeneous counter charge (so-called jellium background) is introduced to neutralize the cell and then to avoid the divergence.[32] This is a popular way to calculate the charged defect energy in traditional three-dimensional (3D) semiconductors.[24]

However, Wang et al.[33] found that applications of the jellium method to charged defects in 2D semiconductors is not as straightforward as the cases in 3D systems. Take boron nitride (BN) as an example in **Figure 2**a; the formation energies of two charged defects [C_N^- (carbon-substituting nitrogen) and C_B^+ (carbon-substituting boron)] in the cases of 2D and 3D BN are calculated. With the increases in the dimension of the supercell in the calculation (i.e., vacuum size L_z for 2D system and volumetric cube root $V^{1/3}$ for 3D system), the formation energies of the charged defect in 3D systems gradually converge to a fixed value, whereas those in the 2D system is almost linearly divergent, see Figure 2a.[33] In other words, the results in 2D materials are strongly dependent on the size of the used supercell, which is definitely illogical from a physical point of view. The veil behind the unphysical phenomenon is uncovered within the schematic diagram of Figure 2b. Jellium charges uniformly distribute in the constructed supercell regardless of the dimension of the system, which is similar to the ionized carriers in the real situation for the 3D system but totally different from that in the 2D system as the ionized carriers in real case are confined in the 2D layer and cannot extend into the vacuum. Due to the weak screening along the vacuum direction, such a distribution leads to strong coulomb interaction between the charged defects and the jellium, as a consequence, the energy of charged defects linearly diverges with increasing vacuum size in the 2D system.[33]

Considerable efforts have been made to overcome the energy divergence for charged defects in 2D semiconductors. Wang et al.[33] developed an efficient scheme by deriving an analytic expression of charged defect energy in a monolayer 2D system as a function of lateral size and vacuum size, with which the converged values can be achieved by doing extrapolation at finite cell sizes. Here, we name the scheme WLZ (Wang, Li, Zhang) method. Since 2D materials with certain thickness such as a few layers or a monolayer on a substrate are much practical

Sha Xia is pursuing a master's degree in the College of Electronic Science and Engineering at Jilin University, China. Her main focus is on the working mechanism in resistive random access memory and defect properties in 2D materials with the first-principles calculations.

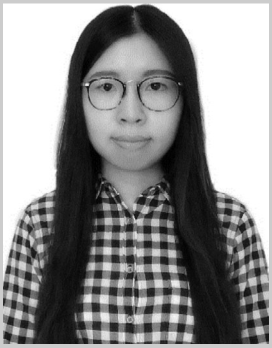

Dan Wang received her B.E. (2011) and Ph.D. (2017) degrees from Jilin University, China. She is now working at Rensselaer Polytechnic Institute, New York. Her research interests lie in developing calculation method for defect evaluation and exploring defect physics in low-dimension materials for technological applications.

Xian-Bin Li received his B.S. (2005), M.S. (2007), and Ph.D. (2010) degrees all in microelectronics from Jilin University, China. He is the professor and the group leader of the Laboratory of Computational Semiconductor Physics in the State Key Laboratory on Integrated Optoelectronics, College of Electronic Science and Engineering, Jilin University. He was also a visiting professor at Rensselaer Polytechnic Institute, New York (2016–2017). Currently, his main focus is on the key problems in microelectronics and optoelectronics with the first-principles calculation, including phase-change memory physics, semiconductor defect physics, and 2D semiconductor design.

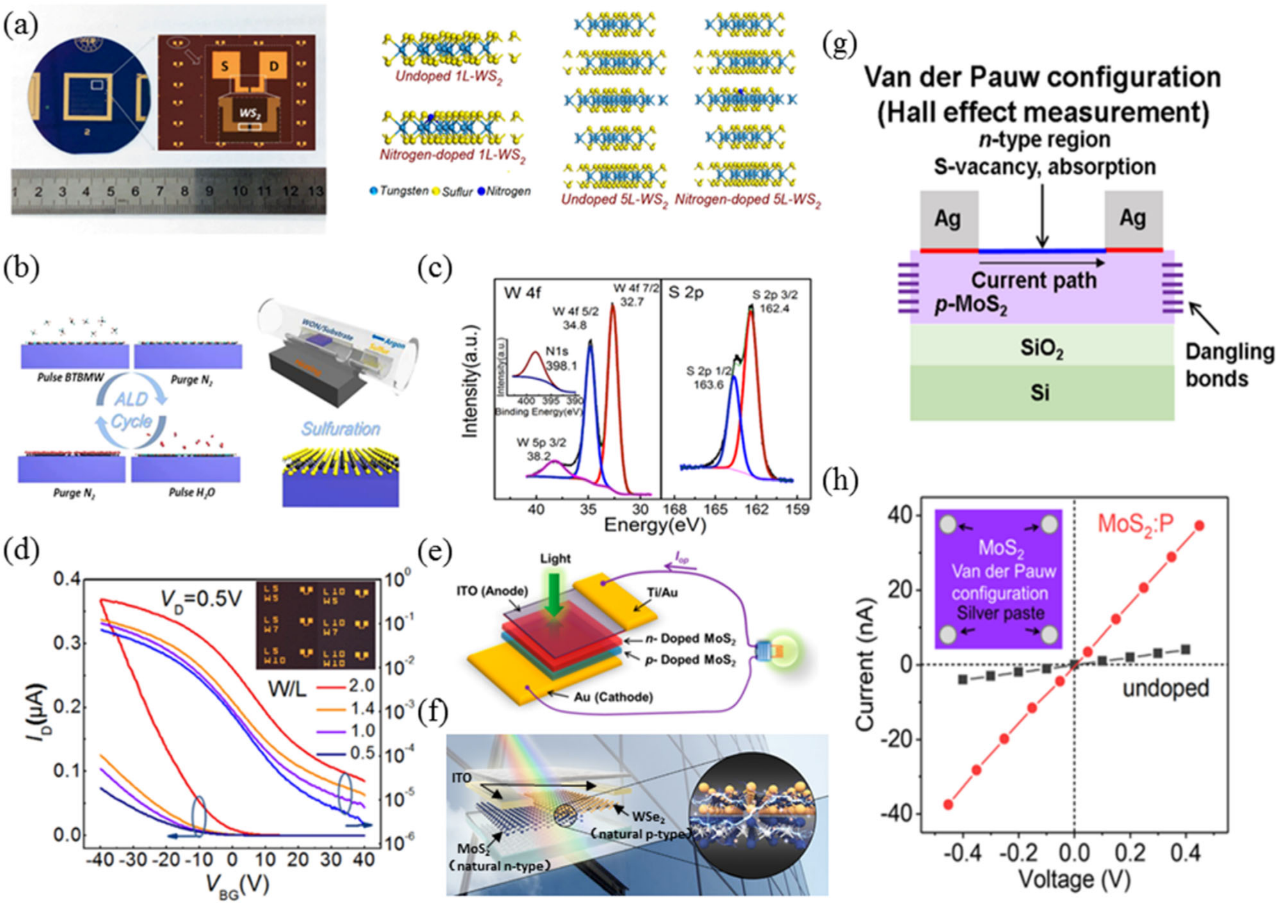

Figure 1. Examples of defect-controlling conductive type in 2D semiconductors for electronic devices. a–d) Stable p-type WS_2 obtained by impurity doping for wafer-level FET device:[27] a) photograph and optical microscopy images of the manufactured WS_2 back-gate FETs on a 2 in. SiO_2/Si wafer. The schematic of atomic models for the undoped and nitrogen-doped WS_2 is also shown; b) synthetic schematic of wafer-scale and layer-controllable WS_2 film on the basis of growth of WO_xN_y film by cycles of atomic layer deposition and then sulfuration; c) XPS spectra to identify W, S, and N elements in the WS_2 films; d) typical transfer characteristics with different W/L (channel width/channel length) for WS_2 FETs. p–n Heterojunction-based photovoltaic solar cell with 2D semiconductors: e) Schematic of PV devices with n/p-doped MoS_2.[29] f) A transparent solar cell with n-type MoS_2/p-type WSe_2 heterojunction.[30] g,h) A vdP device configuration with a p-type MoS_2 with dopant, phosphorous.[31]: g) Schematic illustration of a vdP structure with Ag paste electrodes; h) *I–V* characteristics for the undoped and phosphorous-doped MoS_2 film. a–d) Reproduced with permission.[27] Copyright 2017, American Chemical Society. e) Reproduced with permission.[29] Copyright 2014, American Chemical Society. f) Reproduced with permission.[30] Copyright 2018, American Chemical Society. g,h) Reproduced under terms of the CC-BY licence.[31] Copyright 2018, The Authors, published by AIP Publishing.

in the device applications,[6,11,34–38] Wang et al.[39] further generalized the scheme to 2D systems of arbitrary cell geometry and thickness. The WLZ method is a simple and model-free approach to accurately and efficiently evaluate the formation energy and IE of charged defects in 2D systems, which can be readily invoked. Besides, drawing on the experience of the routine calculation method for charged defects in 3D materials, which is based on the electrostatic energy difference of a model charge in between isolated and periodic boundary conditions, several correction methods for charged defects in 2D and quasi-2D systems have been proposed.[40–45] Since the weak and highly anisotropic screening in 2D systems makes the energy difference calculation much trickier, Sundararaman et al.[46] and Wu et al.[47] unambiguously define an anisotropic dielectric profile, which can be directly derived from regularized density-functional-theory electrostatic potentials, to solve the problem.[46,47]

In this work, we focus on the development of the WLZ extrapolation method and review its application in various defect research in 2D materials. The WLZ formalism for charged defects in monolayer and non-monolayer 2D materials is first addressed, displaying its plausibility and feasibility. Then various defect studies in 2D materials in which IE is calculated within the WLZ method are reviewed, showing the physical pictures uncovered with the calculation method, particularly the defect-level position and its response to surrounding dielectric environments, and unique defect ionization process and its impact on carrier transport. Finally, the review is concluded with an outlook for the potential direction in 2D defect physics. This present review should be useful for researchers to quickly master an efficient tool to evaluate charged defects in 2D materials for the applications in nanoelectronics.

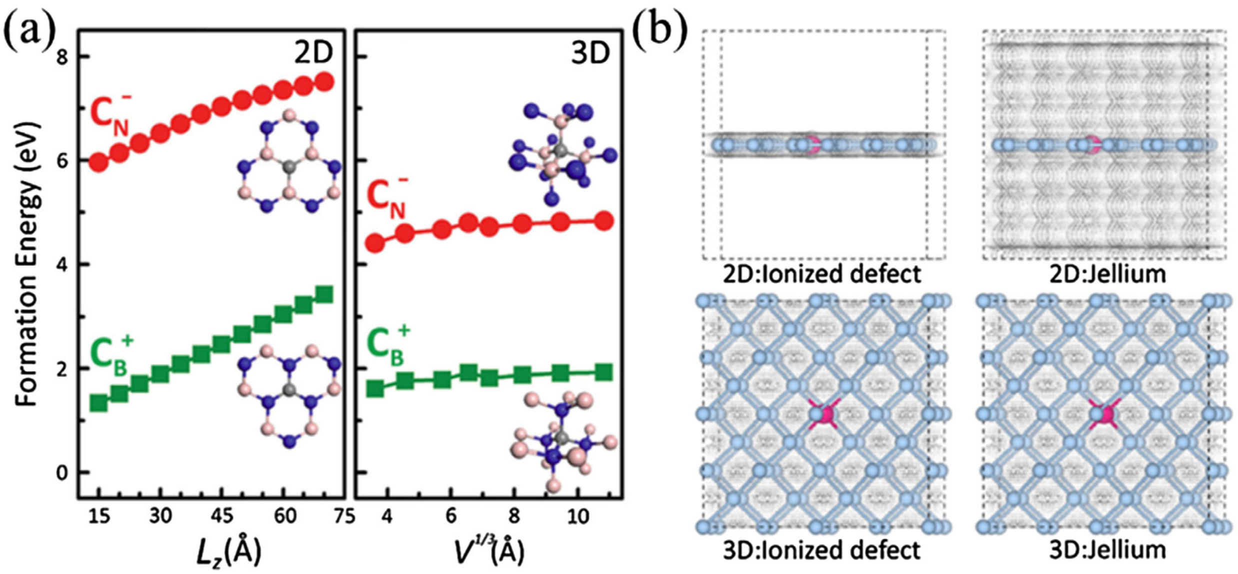

Figure 2. a) Calculated formation energy of charged C_N^- and C_B^+ in 2D BN and 3D BN. Insets illustrate the structure at the vicinity of the defects of BN. Pink, blue, and gray balls represent B, N, and C atoms, respectively. b) Schematic of carrier distribution in real defect ionization and jellium charge distribution in jellium approach of 3D and 2D materials. a) Reproduced with permission.[33] Copyright 2015, American Physical Society. b) Reproduced with permission.[22] Copyright 2017, Elsevier.

2. Energy Prediction of Charged Defects by the WLZ Extrapolation Method

2.1. Fundamentals of Formation Energy of Defects

Under the jellium approach, the formation energy of defect d with charge q can be expressed as[48,49]

$$\begin{aligned}\Delta H_f(q,d) &= E(q,d) - E(host) + \sum_i n_i\mu_i + q(\varepsilon_{\mathrm{VBM}} + \varepsilon_F) \\ &= \Delta E(q,d) + \sum_i n_i\mu_i + q(\varepsilon_{VBM} + \varepsilon_F)\end{aligned} \tag{1}$$

where $E(q,d)$ and E(host) are the total energy of the system with and without defect d, and $\Delta E(q,d)$ is the corresponding energy difference, n_i is the number of atomic species i with chemical potentials μ_i exchanged when the defect is formed. ϵ_{F} is the Fermi energy relative to the valence band maximum (VBM) of the host material ϵ_{VBM}. The defect transition level $\epsilon(q/q')$ is defined as the Fermi energy at which two different charge states (q and q') of the same defect d have the same formation energy, that is, $\Delta H_f(q,d) = \Delta H_f(q',d)$, So,

$$\varepsilon(q/q') + \varepsilon_{VBM} = [\Delta E(q,d) - \Delta E(q',d)]/(q' - q) \tag{2}$$

Using Equation (1) and (2), we can get that $\Delta H_f(q,d) = \Delta H_f(q=0,d) + q[\varepsilon_F - \varepsilon(q/0)]_.$ Note that the formation energy of neutral defect $\Delta H_f(q=0,d)$ can be easily obtained without any corrections in the first-principles calculation, meaning that defect transition energy $\epsilon(q/0)$ has the same divergence with the formation energy of charged defect $\Delta H_f(q,d)$. What is more, calculating $\epsilon(q/q')$ is identical to calculating the IE as IE is the energy difference between $\epsilon(q/q')$ and corresponding band edges (VBM for acceptors and conduction band minimum [CBM] for donors). IE denotes the energy required to excite the electrons/holes from defect levels to band edges to free carriers.[25] According to Boltzmann statistics, the greater the IE, the more difficult it is for the defects to be ionized, and vice versa. The transition level and IE must not diverge with cell size as both are quantities with a clear physical meaning.

2.2. The WLZ Method for Charged Defects in Monolayer 2D Materials

Wang et al. used classical electrostatics to understand the energy divergence of the charged defect with cell sizes as mentioned earlier.[33] In the limit of vacuum size L_z approaching infinity at fixed lateral size L_s ($=L_x = L_y$), namely $L_z >> L_s$, the system can be considered as a continuum charged plane in a uniform jellium charge background. The electrostatic energy of the system is dominated by the interaction between them and is demonstrated to be

$$E_{tot} = \frac{q^2}{24\sin\theta L_s^2\varepsilon_0}L_z = \frac{\beta' L_z}{L_s^2}\left(= \frac{q^2}{24S\varepsilon_0}L_z = \frac{\beta L_z}{S}\right) \tag{3}$$

where S is the area of the 2D slab and θ is the angle between L_x and L_y ($L_x = L_y$ for current case).

The L_z dependence well explains the linear divergence of the formation energy of a charged defect with increasing L_z. The slope of the divergent formation energy agrees well with that in the electrostatic model, that is, $\frac{\beta}{S}$. In addition, another L_z-independent term $\frac{\alpha}{\sqrt{S}}$ is invoked to correct the nonuniformity of the planar charge for real systems, where α is the Madelung constant.[50] The cell-size-dependent IE(S, L_z)for the defect is, therefore, in the asymptotic form

$$\mathrm{IE}(S, L_z) = \mathrm{IE}_0 + \frac{\alpha}{\sqrt{S}} + \left(\frac{\beta}{S}\right) L_z \tag{4}$$

where IE_0 is the true, size-independent IE.

To be more rigorous, they also obtained Equation (4) by expanding IE(L_s, L_z) in a power series of $L_s(=L_x = L_y)$ and L_z, $IE(L_s, L_z) = \sum_{i,j=-\infty}^{\infty} c_{i,j} L_s^i L_z^j$, and then removing irrelevant coefficients through taking three physical limits: 1) $L_z \to \infty$ at fixed L_s; 2) $L_s \to \infty$ at fixed L_z; and 3) $L_s = L_z \to \infty$, for all of which the cell-size dependence of the electrostatic energy can be derived. The resultant power expansion is reduced to

$$\begin{aligned} IE(L_s, L_z) = {} & \frac{1}{L_z}\left\{ t\ln(L_x) + c'_{0,-1} + \frac{c'_{-1,-1}}{L_x} + \cdots \right\} \\ & + \left(\frac{c_{-1,0}}{L_s} + IE_0\right) + L_z \frac{c_{-2,1}}{L_s^2} \end{aligned} \tag{5}$$

By maintaining $L_z >> L_s$, the first term can be ignored and then the expression arrives at Equation (4), namely

$$IE(L_s, L_z) = \left(\frac{c_{-1,0}}{L_S} + IE_0\right) + L_z \left(\frac{c_{-2,1}}{L_s^2}\right) = IE_0 + \frac{\alpha}{\sqrt{S}} + \frac{\beta L_z}{S} \tag{6}$$

The result obtained with the method is in good agreement with the additional benchmark calculation where the converged energy is achieved by extrapolating the linear dependence of the divergent energy on $1/L$ to $L \to \infty$ with super large $L = L_x = L_y = L_z$. Apart from the accuracy of the method, the efficiency has also been demonstrated as the unknown parameter α is proved to be mainly dependent on the geometry of the 2D materials, but not on the specific defect.

2.3. The Updated WLZ Method for 2D Materials with Arbitrary Thickness

2D materials are highly sensitive to external environments, which makes engineering the dielectric surroundings a powerful way to modify their properties and the performance of the devices based on them.[7,51,52] It has been experimentally reported that using high-k substrate such as HfO_2 can enhance the mobility of the MoS_2 transistor.[53] On the other hand, 2D materials are usually not free-standing during the processes of material growth, experimental characterization, property measurement, and device fabrication. So, a critical point to the advancement of the 2D microelectronics is the abundant understanding of charged defects in 2D systems with certain thickness such as few-layer 2D and 2D material on a substrate. However, straightforwardly applying the monolayer formalism above to thicker 2D systems would require large enough vacuum size, making the calculations laborious.

To address the issue, Wang et al.[39] further derived a general formalism for charged defects in 2D systems with arbitrary thickness. Starting with the power expansion of $IE(L_x, L_z) = \sum_{i,j=-\infty}^{\infty} c_{i,j} L_x^i L_z^j$, they revisited the first physical limit of $L_z \to \infty$ at fixed $L_x (L_y = \gamma L_x)$ in which the system can be regarded as a charged slab with area $S = L_x \times L_y \times \sin\theta = \gamma {L_x}^2 \sin\theta$ and thickness $2d_0$ immersed in jellium background charges. In this case, the total electrostatic energy is

$$\begin{aligned} E_{\text{total}} = {} & \frac{q^2}{24\gamma L_x^2 \epsilon_0 \sin\theta}\left[(L_z - 4d_0) - 2d_0\left(1 - \frac{1}{\epsilon_\perp}\right)\right] \\ & + \frac{q^2 d_0^3}{3\gamma L_x^2 \epsilon_0 \sin\theta}\left(\frac{1}{\epsilon_\perp} - 1\right)\frac{1}{L_z^2} \\ & + \frac{q^2 d_0^2}{4\gamma L_x^2 \epsilon_0 \sin\theta}\left(2 - \frac{4}{3\epsilon_\perp}\right)\frac{1}{L_z} \end{aligned} \tag{7}$$

where ϵ_0 is the vacuum dielectric constant and $\epsilon_\perp$ is the out-of-plane relative dielectric constant of the 2D material. The energy now depends on L_z^{-2}, L_z^{-1}, L_z^0, and L_z^1, of which the former two contribute more with increasing slab thickness ($2d_0$). This tendency has also been validated by their calculations on the IE of $\mathrm{Te_P}$ (one Te atom substituting one P atom) in monolayer, bilayer, and trilayer black phosphorus (BP) as shown in **Figure 3**a.[39] Obviously, the contribution of terms L_z^{-2} and L_z^{-1} to IE follows the sequence of trilayer > bilayer > monolayer at smaller L_z whereas the L_z^1 dominates the energy in larger L_z for all three cases. Keeping all the terms of which the divergence is not slower than L_z^{-2} and L_x^{-2}, the reduced power expansion of $IE(L_x, L_z)$ is

$$\mathrm{IE}(L_{x,} L_z) = \frac{c_{0,-2}}{L_z^2} + \frac{c(L_x)}{L_z} + \left(\frac{c_{-2,0}}{L_x^2} + \frac{c_{-1,0}}{L_x} + \mathrm{IE}_0\right) + L_z\left(\frac{c_{-2,1}}{L_x^2}\right) \tag{8}$$

where $c(L_x) = t\ln(L_x) + c'_{0,-1} + \frac{c'_{-1,-1}}{L_x}$.

They proposed two methods to get IE_0 since it is tricky to directly fit all parameters in Equation (8). For the first one, they defined $\overline{\overline{IE(L_x, L_z)}}$ as

$$\begin{aligned} \overline{\overline{\mathrm{IE}(L_x, L_z)}} & = \mathrm{IE}(L_x, L_z) - \frac{c_{0,-2}}{L_z^2} - \frac{c(L_x)}{L_z} - L_z\left(\frac{c_{-2,1}}{L_x^2}\right) \\ & = \frac{c_{-2,0}}{L_x^2} + \frac{c_{-1,0}}{L_x} + \mathrm{IE}_0 \end{aligned} \tag{9}$$

The right hand of the equation contains IE_0, $\frac{1}{L_x}$, and $\frac{1}{L_x^2}$, playing the same role with the term L_z^0, which therefore can be obtained by fitting $IE(L_{x,} L_z)$ as a function of L_z^n ($n \in [-2, 1]$) at fixed L_x. For different L_x, the value is definitely different, as shown in Figure 3b, enabling one to get IE_0 by extrapolating $\overline{\overline{IE(L_x, L_z)}}$ at the diverse L_x back to $1/L_x \to 0$.

To further reduce the computational cost, they came up with the second way where the L_z^{-2} and L_z^{-1} are both ignored at finite L_z and then Equation (8) changes to

$$IE\left(L_x, L_z\right) = \frac{c_{-2,0}}{L_x^2} + \frac{c_{-1,0}}{L_x} + IE_0 + L_z\left(\frac{c_{-2,1}}{L_x^2}\right) \tag{10}$$

with $c_{-2,0} = \frac{q^2}{24\gamma\varepsilon_0 \sin\theta}[-4d_0 - 2d_0(1 - \frac{1}{\varepsilon_\perp})]$ and $c_{-2,1} = \frac{q^2}{24\gamma\varepsilon_0 \sin\theta}$

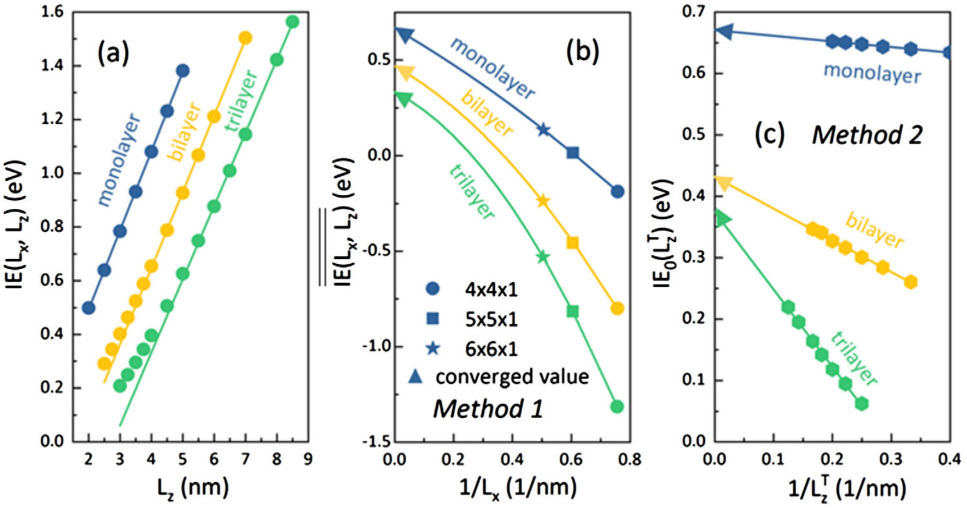

Figure 3. a) IE (L_x, L_z) of Te_P in monolayer (ML), bilayer (2L), and trilayer (3L) BP, respectively. The converged ionization energy of Te_P in ML, 2L, and 3L BP, in panel (b), by method 1 and in panel (c), by method 2. The blue, orange, and green arrows represent the real ionization energy IE$_0$s in ML, 2L, and 3L, respectively. a–c) Reproduced with permission.[39] Copyright 2017, American Physical Society.

Then one can get $IE_0(L_z^T)$ as a function of L_z^T (at which the L_z^{-2} and L_z^{-1} are neglected) and true IE$_0$ is the intercept of $IE_0(L_z^T)$ at $L_z^T \to \infty$. Figure 3c shows the $IE_0(L_z^T)$ of Te_P in monolayer, bilayer, and trilayer BP. It can be evidently seen that the slope becomes steeper with increasing layer number, which once again indicates the more and more contribution from terms L_z^{-2} and L_z^{-1} for thicker and thicker 2D systems. The true IE$_0$s in method 2 are well consistent with that in method 1, with an energy tolerance of 30–40 meV. Overall, the WLZ method makes it possible to reliably predict defect energies and transition levels in 2D materials, and Equation (4) is suitable for monolayer systems and Equation (9) and (10) are recommended for multilayer or monolayer on a substrate.

3. Applications of the WLZ Method: Defect Physics in Various 2D Materials

The WLZ method enables the community to reliably calculate IEs of defects in any 2D materials, making it possible to explore the defect physics in low dimension. Next, we will review recent advances in defect studies for popular 2D materials (including BN, MoS_2, BP, and InSe) where the WLZ method is adopted to obtain convergent energies and highlight the unique physical pictures induced by the dimensionality reduction. Note that the WLZ method applies to any functionals. It is well known that density functional theory underestimates band gap[54] and the many-body perturbation theory is demonstrated to be reliable in predicting band gap.[55] Hence, the choice of functional would significantly affect the evaluation of defect IE[45,47,56] as it is the energy distance between the defect transition level and the band edge.

3.1. Defect Ionization Energies in Popular 2D Materials

IE is an extremely important quantity for 2D materials in multiple technological applications. It determines the ability of one defect to supply carriers and requires being small for ideal conductivity in electronics. On the contrary, quantum defects seek large IE to preclude resonance of the defect levels with bulk band edges for long coherence time. The fast development of 2D materials in electronics and quantum technologies has promoted the theoretical prediction of IE of various defects in 2D materials. For example, Wang et al.[33] studied the transition level of C_B, C_N, V_B (boron vacancy), and V_N (N vacancy) in monolayer hexagonal BN, as shown in **Figure 4**. C_B and V_N are donors with transition levels $\varepsilon(+1/0)$ being $\varepsilon_{CBM} - 2.03$ eV and $\varepsilon_{CBM} - 2.50$ eV, and C_N and V_B are acceptors with transition levels $\varepsilon(0/-1)$ being $\varepsilon_{VBM} + 1.86$ eV and $\varepsilon_{VBM} + 1.44$ eV, respectively. The deep characteristic of the defects implies the weak ability to ionize carriers. However, the ability is significantly increased in 3D cubic BN with IE of 0.00 eV for C_B, 0.36 eV for V_N, 0.18 eV for C_N, and 0.37 eV for V_B.

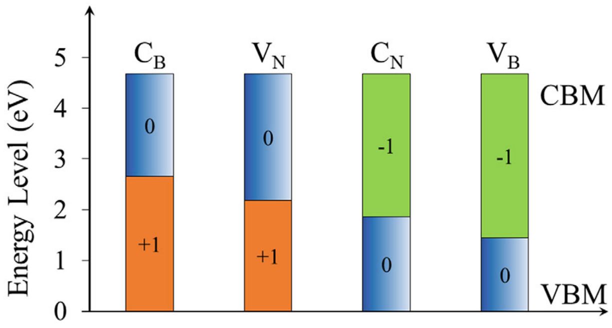

Figure 4. Stable charge states and transition levels of donors (C_B, V_N) and acceptors (C_N, V_B) in monolayer BN. Data taken from Ref. [33].

The more popular 2D materials used as the channel material in electronic devices, such as the FET, are the transition metal dichalcogenide (especially MoS_2) and BP.[6,7,57–60] MoS_2 naturally shows n-type electrical conductivity without intentional doping[30,53,61,62] and the origin is usually assigned as the most often observed V_S (sulfur vacancy). Wang et al.[63] calculated the formation energies of six native defects in charge states of (2−),

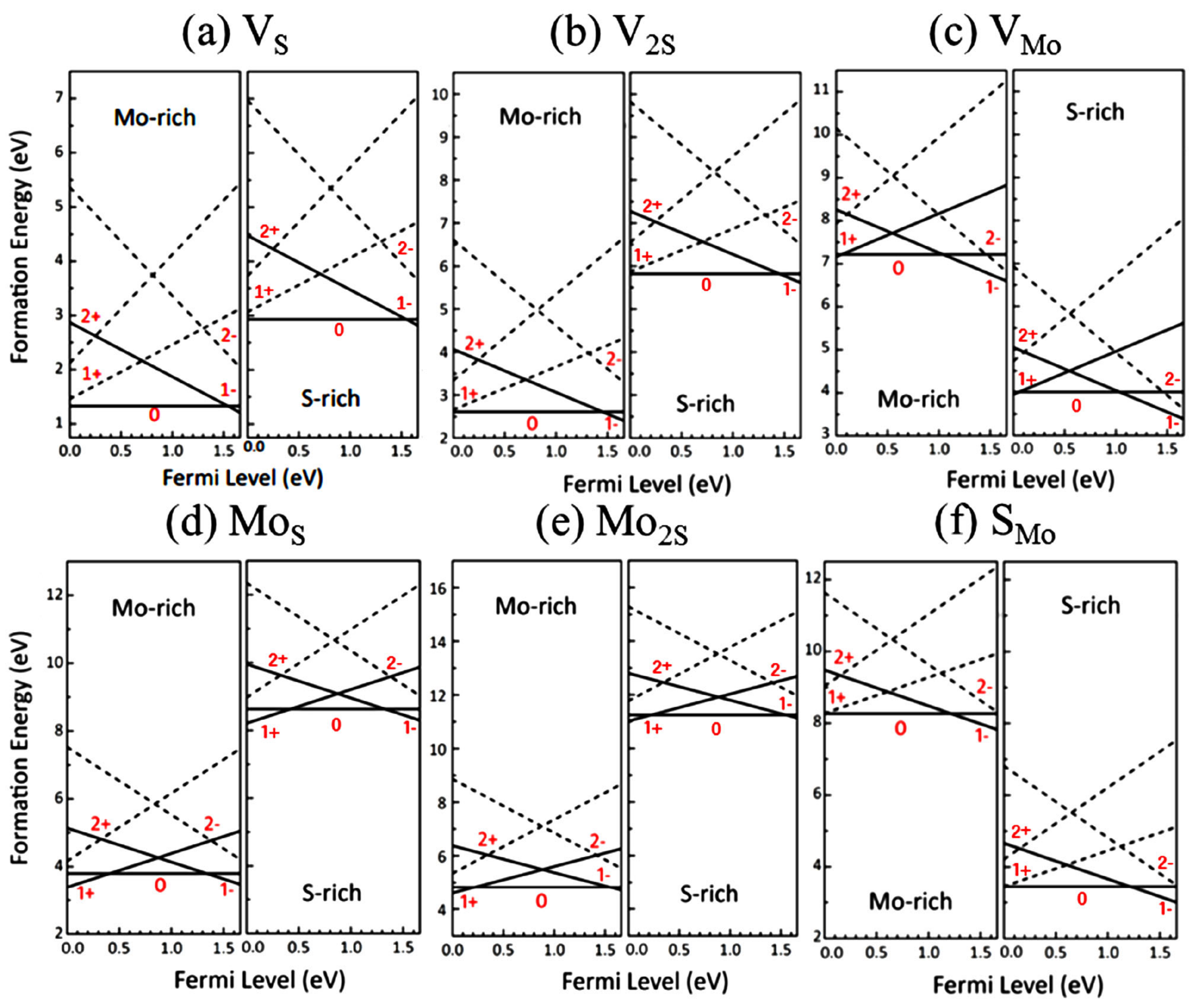

Figure 5. Formation energies of native defects in monolayer MoS_2. a) V_S, b) V_{2S} (double S vacancy), c) V_{Mo} (Mo vacancy), d) Mo_S (antisite, one Mo substituting one S atom), and e) Mo_{2S} (one Mo substituting two S atoms), and f) S_{Mo} (antisite, one S substituting one Mo atom). (a–f) Reproduced under terms of the CC-BY licence.[63] Copyright 2019. The Authors, published by Springer Nature.

(1−), (0), (1), and (2) as shown in **Figure 5**. V_S, V_{2S}, Mo_S, and Mo_{2S} have lower formation energies under Mo-rich condition, whereas V_{Mo} and S_{Mo} have lower formation energies under S-rich condition. V_S has the lowest energy among all the native defects that agree with the experimental observation.[64,65] The stable charge states of V_S, V_{2S}, and S_{Mo} are found to be (0) and (1−) and those of V_{Mo}, Mo_{2S}, and Mo_S are (1+), (0), and (1−), when the Fermi level is inside the band gap. The most likely charge-state transition is from (0) to (1−) for acceptors V_S, V_{2S}, S_{Mo}, and V_{Mo} with corresponding IEs being 1.55, 1.45, 1.22, and 1.04 eV, and from (0) to (+1) for donors Mo_S and Mo_{2S} with respective IEs being 1.24 and 1.44 eV. Obviously, V_S is a deep acceptor, which means that it is not the source of the n-type conductivity of MoS_2. Neither are the donor-type native defects, Mo_S, and Mo_{2S}, due to their deep levels. Another possibility for the natural n-type conductivity is Re impurity that is often contained in MoS_2 sample. They reported that though Re_{Mo} (one Re atom substituting one Mo atom) has a deep level at 0.45 eV below the CBM, it still can greatly contribute to the n-type conductivity via the charged-defect-bound carriers instead of the free carriers as in 3D materials. The details would be discussed in Section 3.3 for the Re-bound carriers.

The problem of doping asymmetry not only exists in MoS_2 but also spreads to BP, for which p-type conductivity can be obtained rather easily than n-type.[6,7,66–68] To explore the n-type doping possibility of BP, Wang et al.[39] studied the native defects (vacancy V_P and interstitial P_i) and group-VI element substitution (O, S, Se, and Te) in monolayer BP. **Figure 6** shows the optimized atomic structure and the formation energies of the defects. Neutral V_P and P_i have larger formation energies with considerable atomic distortion. They are both acceptors with transition level being $\varepsilon_{VBM} + 0.36$ eV and $\varepsilon_{VBM} + 0.48$ eV, respectively. For the group-VI elements O, S, Se, and Te, they form two bonds with adjacent P atoms in the bottom layer, leaving one dangling bond of the P

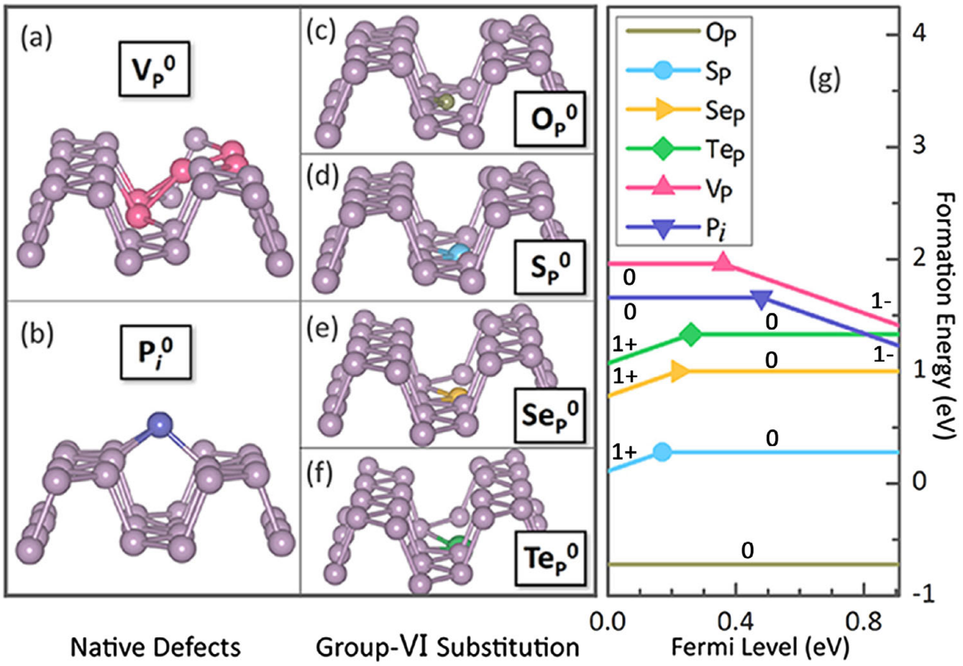

Figure 6. a–f) Atomic configuration and g) formation energies of native defects V_P and P_i and substitutional defects O_P, S_P, Se_P, and Te_P in monolayer BP. The Fermi level ranges from VBM (set to zero) to CBM (equals to the bandgap, 0.91 eV). a–g) Reproduced with permission.[39] Copyright 2017, American Physical Society.

atom in the top layer and therefore are all donors. Among them, O_P has the lowest neutral formation energy of −0.72 eV. It means O is incredibly easy to be doped in BP, which is in line with the high sensitivity of BP to air. The donor levels of S_P, Se_P, and Te_P are within the band gap, being 0.74, 0.69, and 0.67 eV below the CBM whereas that of O_P is outside the band gap, 0.11 eV below the VBM. Hence, the best candidate for n-type doping is Te_P with IE of 0.67 eV. Though it is too deep to supply enough carriers at room temperature, their subsequent calculations show that the IE decreases by half (to 0.33 eV) in trilayer BP due to the increased screening. More discussions about the dielectric screening effect on defects in 2D materials can be found in Section 3.2.

Apart from MoS_2 and BP, 2D InSe has recently sparked great interest in the scientific community as the devices based on it display higher carrier mobility than MoS_2[69,70] and stronger stability than BP.[70–73] Wang et al.[74] conducted a systematic evaluation on the properties of native defects (vacancy V_{In} and V_{Se}) and substitutional dopants (X_{In}, X = Zn, Cd, Hg, Ge, Sn, and Pb and X_{Se}, X = As, Sb, Bi, Cl, Br, and I) in monolayer InSe. **Figure 7**a–d show the band structure of Zn_{In}, Ge_{In}, As_{Se}, and Cl_{Se} (as representatives for respective group-IIB, group-IVA, group-VA, and group-VIIA elements as the same group elements have similar electronic structure). For Zn_{In} and As_{Se}, one occupied spin-up state denoted by 1 and one unoccupied spin-down state denoted by 2 are induced in the band gap. The states are close to VBM and far from CBM. It is much easier for state 2 to accept one electron from VBM than state 1 to donate one electron to CBM. So, Zn_{In} and As_{Se} are acceptors. Likewise, Ge_{In} is a donor. For Cl_{Se}, the excess electron of Cl than Se resides in the CBM, implying a shallower nature. The impurity states mainly come from the dopant elements and surrounding host atoms as shown in Figure 7e–h.

The carrier type and density can be qualitatively determined from the above single-particle electronic structures, but the quantitative evaluation needs the calculations of IE. Figure 7i–l shows the formation energies of the defects in neutral and charged states (+1 for donors and −1 for acceptors) as a function of Fermi energy varying from VBM to CBM and atomic chemical potential depending on the growth conditions of the sample materials, such as In-rich conditions or Se-rich conditions. The In-related defects (V_{In} and X_{In}) and Se-related defects (V_{Se} and X_{Se}) are likely to be formed under Se-rich conditions and In-rich conditions, respectively. V_{Se} is an electronically inactive defect as there is only one stable state (0) and no charge state transition when the Fermi level is within the bandgap. V_{In} is a deep acceptor with transition level being 0.74 eV above the VBM. The extrinsic dopants, X_{In} (X = Zn, Cd, and Hg), X_{Se} (X = As, Sb, and Bi), X_{In} (X = Ge, Sn, and Pb), and X_{Se} (X = Cl, Br, and I) are all deep acceptors or donors with IE in the range of 0.41–0.84 eV. It should be noted that the Kohn–Sham levels often fail to capture the defect nature. Taking X_{Se} (X = Cl, Br, and I) as examples, the band structure of Figure 7d shows they are extremely shallow donors. However, their IEs are found to be as large as 0.46, 0.47, and 0.51 eV, demonstrating the necessity of IE calculation for defect evaluation.

3.2. Dielectric Screening Effect on Defect in 2D Materials

Defects in 2D materials are usually deep,[33,51,75] causing troubles to achieve desired free carriers[76] and then limiting their application in electronic devices. The deep nature originates

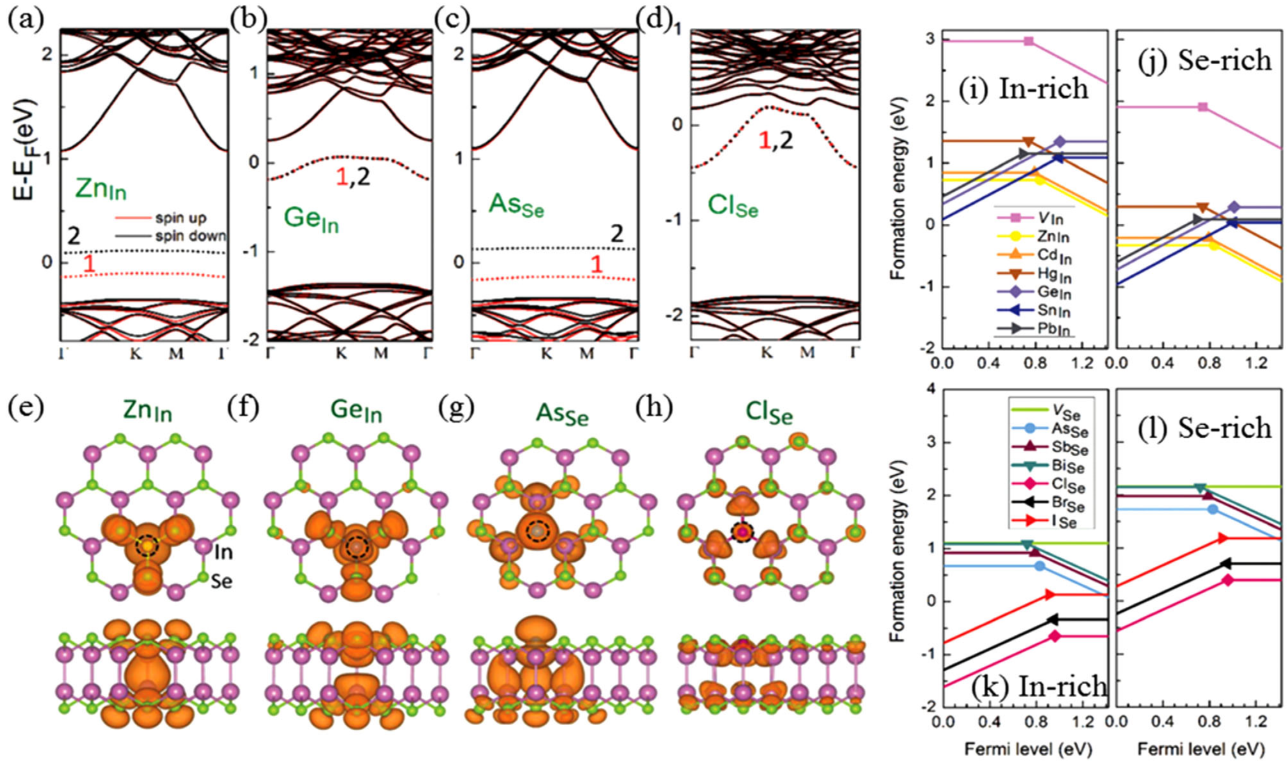

Figure 7. The spin-polarized band structures and the charge density distributions of a,e) Zn_{In}, b,f) Ge_{In}, c,g) As_{Se}, and d,h) Cl_{Se} as respective representatives for group-IIB, group-IVA, group-VA, and group-VIIA dopants. The dashed circles in the charge density distribution maps denote the positions of the defects. The converged formation energies as a function of the Fermi level for all the defects under i,k) In-rich conditions and j,l) Se-rich conditions. a–l) Reproduced with permission.[74] Copyright 2017, The Royal Society of Chemistry.

from the weak screening in 2D materials, which leaves the charged defect alone and close to a bare charge. As a result, the charged formation energy and IE (defined as the energy difference between charged and neutral formation energies) are both increased substantially. What one can get from this is that modification of the dielectric environments surrounding the 2D materials would have a profound effect on the defect properties.[77]

As mentioned above, Te_P has a deep IE of 0.67 eV in monolayer BP. By increasing the layer number, Wang et al.[39] found that the IE decreases to 0.47 eV in bilayer BP and further to 0.33 eV in trilayer BP, as shown in **Figure 8**a. This tendency is further evidenced by the increasingly more delocalized charge density distribution of the defect level as shown in Figure 8b. The spatial charge distribution in X and Y direction (in the plane) significantly reduces at Te site but increases at the tail region far away from Te site. In the Z direction perpendicular to the plane, the charges extend into the second atomic layer for the bilayer and the trilayer BP, which also can be seen from the charge plot in the inset of Figure 8a. The variation of the charge density distribution is more from monolayer to the bilayer BP, agreeing well with the IE reduction tendency.

The dielectric environment effects on defect were reported in MoS_2 as well. Using the WLZ method, Ma et al.[78] calculated the IEs of X_S (X = Cl, Br, and I) in free-standing MoS_2 and MoS_2 with substrates (SiO_2 and Al_2O_3), as shown in **Figure 9**. Two inequivalent doping sites are considered, namely the outer-layer and inner-layer sites, which mean that the substitution doping happens in the S atomic layer exposed into the vacuum and the substrates, respectively. It is shown that the IEs decrease from MoS_2 to MoS_2/SiO_2 and further to MoS_2/Al_2O_3 as a result of increased screening, demonstrating a valid route to tune defect IE by substrate engineering. Specifically, the IE of I_S decreased from 0.63 eV in free-standing MoS_2 to 0.39 eV in MoS_2/SiO_2 and further to 0.17 eV in MoS_2/Al_2O_3 for the inner-layer doping sites. For the outer-layer doping site, the IE of I_S increased to 0.39 eV in MoS_2/Al_2O_3. This can be understood as the outer-layer doping site is farther from Al_2O_3 and then captures weaker screening. The different screening effects for inner-doping and outer-doping sites can also be described by the charge density spatial distribution of the defect level, as shown in Figure 9b. The charge density for the outer-layer doping site is more localized than that for the inner-layer one.

The results of the dielectric screening effects on defects in 2D materials open up new possibilities in the field of defect engineering for device design. On the other hand, the dielectric surroundings are very vital for 2D materials that are often not free-standing in most practical applications. So, a sufficient understanding of the screening effects is imperative for the development of 2D electronics. On the other hand, the WLZ method can help to capture this critical physics in 2D materials.

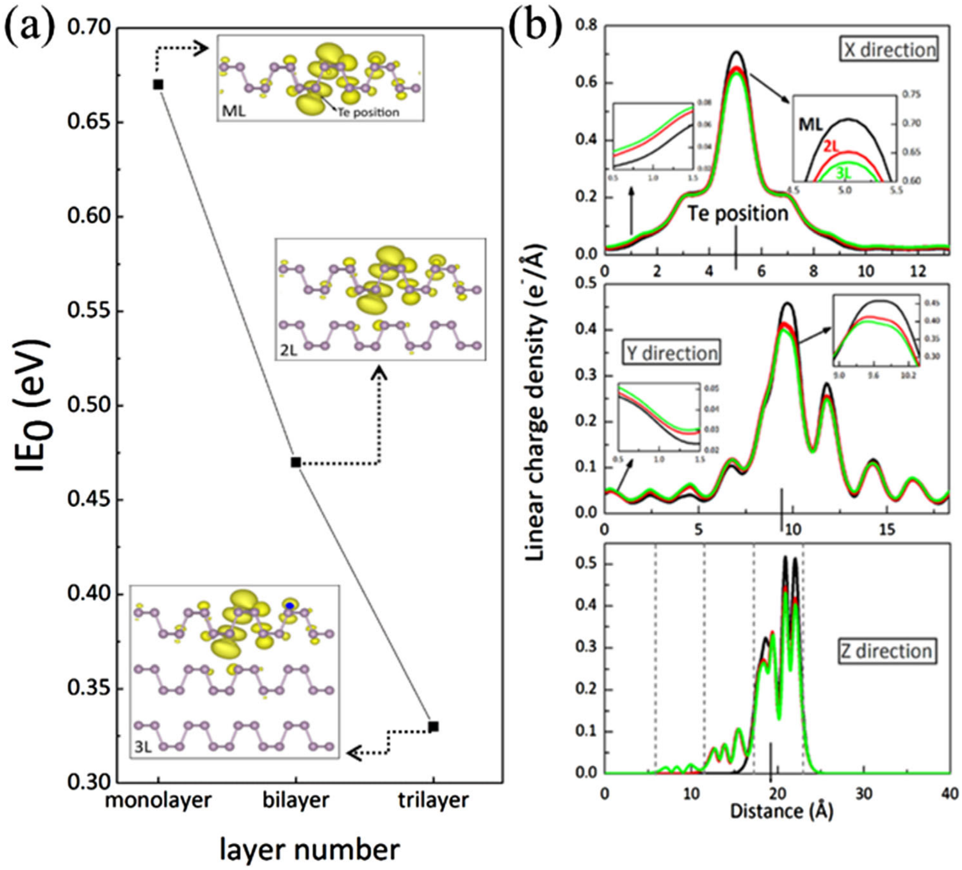

Figure 8. a) Converged ionization energy of Te_P in monolayer, bilayer, and trilayer BP. Insets show the charge contour plots of the donor level of Te_P. b) The non-averaged linear charge density of the defect level of Te_P along with the in-plane and out-of-plane directions in monolayer, bilayer, and trilayer BP, respectively. The vertical black solid line represents the position of the Te impurity. a,b) Reproduced with permission.[39] Copyright 2017, American Physical Society.

3.3. Unique Defect Ionization Picture and Carrier Transport in 2D Materials

Though the defects are found to be deep in 2D materials from the theoretical point of view, a certain extent of n-type or p-type conductivity has been experimentally observed.[53,79–82] The discrepancy can be addressed with the unique defect ionization process and carrier transport mechanism in 2D materials that are reported by Wang et al.[63] with the WLZ method. Due to the quantum confinement and reduced screening in 2D materials, when the electron or hole on defect level is ionized to the band edges, it is still bound by the positively or negatively charged defect, and extra energy is required to overcome the binding energy and then truly free the carriers. This means that IE in 2D is composed of two parts, one of which (IE_1) is used for exciting the carrier to the defect-bound-band-edge (DBBE) states and the other of which (E_{db}) is the coulomb-binding energy between the charged defects and the ionized carriers, namely, $IE = IE_1 + E_{db}$. The DBBE states are demonstrated to become localized with increased E_{db} for various defects in MoS_2. Importantly, the DBBE states can be a special way for carrier transport. **Figure 10**a,b shows the band structure of MoS_2 and Re-doped MoS_2. The extra electron of Re spontaneously occupies the CBM, forming the DBBE state and meaning $IE_1 = 0$ eV. Recalling the large IE of 0.45 eV of Re_{Mo} in monolayer MoS_2 mentioned above, then the $E_{db} = IE_0 = 0.45$ eV. The wavefunction of the DBBE state tends to overlap, as shown in Figure 10c,d, which can facilitate carrier transport. Moreover, the overlap can be strengthened by increasing the surrounding screening such as substrates. Therefore, the experimental conductivity measurement of doped MoS_2 could be, as a matter of fact, a special case of DBBE-state transport.

4. Conclusions and Outlooks

In summary, the fundamentals of the WLZ extrapolation method and its important role in evaluating the charged defects in 2D materials and revealing the associated defect physics in 2D dimensions have been reviewed in this work. The WLZ method distinguishes itself by featuring no empirical parameters and applies to any functionals. Particularly, the IE of various defects in popular 2D materials obtained with the WLZ scheme, the dielectric screening effects on charged defects, together with the identification of defect-bound-band-edge states and their significant influences on the defect ionization process and carrier transport mechanism are highlighted. This review advances the

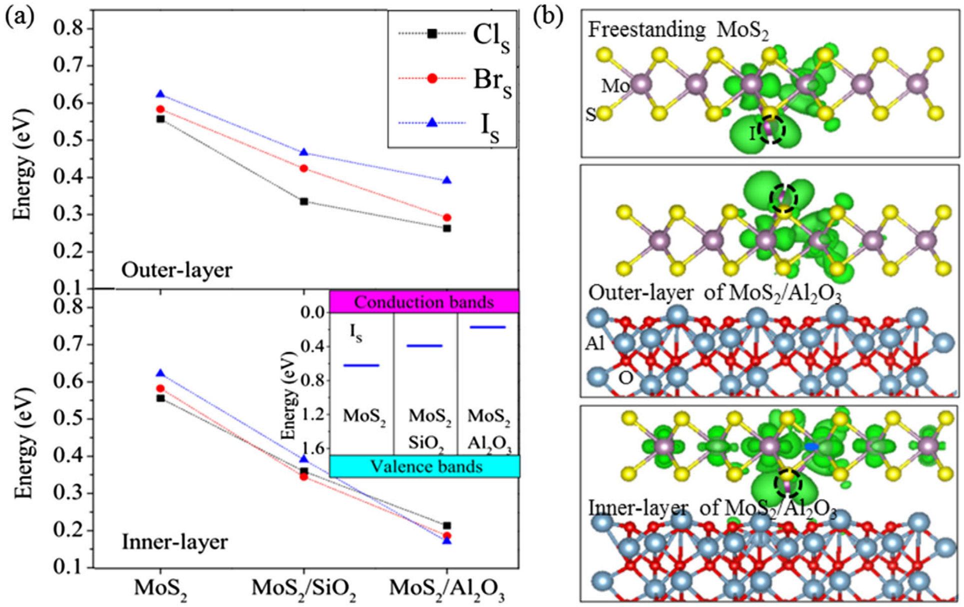

Figure 9. a) Calculated IEs for the X_S (X = Cl, Br, I) in free-standing MoS_2, MoS_2/SiO_2, and MoS_2/Al_2O_3. Top for inner-layer doping sites and bottom for outer-layer doping sites. Inset shows the IE positions of the inner-layer I_S within the band gap. b) The charge density for I_S in the free-standing MoS_2, MoS_2/Al_2O_3 with inner-layer and outer-layer doping sites. The light purple, yellow, light blue, red, and purple balls denote Mo, S, Al, O, and I atoms, respectively. The green surface indicates the dopant charge. Dashed circles represent the positions of the dopant I. a,b) Reproduced with permission.[78] Copyright 2017, American Physical Society.

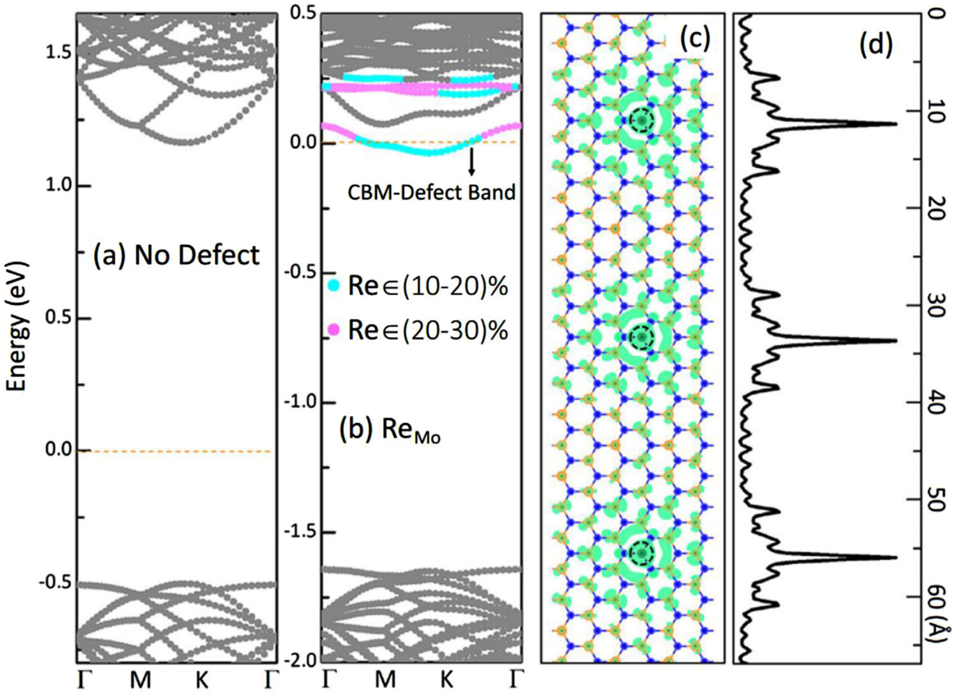

Figure 10. Band structure of a) perfect and b) Re-doped monolayer MoS_2 with a defect density of $\approx 10^{13}$ cm^{-2}. The spatial distribution of the charged defect bound band c) and its corresponding linear charge density d). Dashed circles represent the defect locations. The isosurface in panel (c) is 3×10^{-4} $e/a_0{}^{-3}$, where a_0 is the Bohr radius. a–d) Reproduced under terms of the CC-BY licence.[63] Copyright 2019. The Authors, published by Springer Nature.

understanding of 2D defect physics. Though the high level of interest in defects of 2D materials, combined with the development of computational method, has led to an outburst of defect studies and then rapid progress in this field over the past years, the defect evaluation for promoting the industrial evolution of 2D nanoelectronics is still facing challenges. The subsequent research on the following several topics would be useful: 1) further development of evaluation method toward huge savings in computational cost especially for the multilayer, heterostructure, and complex systems with various dielectric environments; 2) the exploration of how the defect energies respond to the theory level; and 3) the construction of database of defect properties by high-throughput calculations. Finally, the semiconductor companies, such as Taiwan Semiconductor Manufacturing Company, have started to consider the possibility of 2D materials for integrated circuit manufacturing to extend Moore's law;[16] we expect the WLZ extrapolation method can help to analyze defect physics for various 2D materials in time to the semiconductor community.

Acknowledgements

S.X. and D.W. contributed equally to this work. This work was supported by the National Natural Science Foundation of China (No. 11874171, No. 61922035, and No. 11904118). The details of the WLZ method can be found in the website of https://2d-defect-ee.weebly.com/.

Conflict of Interest

The authors declare no conflict of interest.

Keywords

2D semiconductors, carrier transport mechanisms, charged defect, dielectric environment effect, WLZ extrapolation

Received: July 15, 2019
Revised: November 16, 2019

---

[1] K. S. Novoselov, A. K. Geim, S. V. Morozov, D. Jiang, Y. Zhang, S. V. Dubonos, I. V. Grigorieva, A. A. Firsov, *Science* **2004**, *306*, 666.
[2] Q. H. Wang, K. Kalantar-Zadeh, A. Kis, J. N. Coleman, M. S. Strano, *Nat. Nanotechnol.* **2012**, *7*, 699.
[3] M. Xu, T. Liang, M. Shi, H. Chen, *Chem. Rev.* **2013**, *113*, 3766.
[4] D. Pacile, J. Meyer, Ç. Girit, A. Zettl, *Appl. Phys. Lett.* **2008**, *92*, 133107.
[5] J. Qiao, X. Kong, Z.-X. Hu, F. Yang, W. Ji, *Nat. Commun.* **2014**, *5*, 4475.
[6] L. Li, Y. Yu, G. J. Ye, Q. Ge, X. Ou, H. Wu, D. Feng, X. H. Chen, Y. Zhang, *Nat. Nanotechnol.* **2014**, *9*, 372.
[7] H. Liu, A. T. Neal, Z. Zhu, Z. Luo, X. Xu, D. Tománek, P. D. Ye, *ACS Nano* **2014**, *8*, 4033.
[8] A. Pospischil, M. M. Furchi, T. Mueller, *Nat. Nanotechnol.* **2014**, *9*, 257.
[9] F. Xia, H. Wang, D. Xiao, M. Dubey, A. Ramasubramaniam, *Nat. Photonics* **2014**, *8*, 899.
[10] K. F. Mak, J. Shan, *Nat. Photonics* **2016**, *10*, 216.
[11] S. B. Desai, S. R. Madhvapathy, A. B. Sachid, J. P. Llinas, Q. Wang, G. H. Ahn, G. Pitner, M. J. Kim, J. Bokor, C. Hu, H. Philip Wong, A. Javey, *Science* **2016**, *354*, 99.
[12] C. Tan, Z. Liu, W. Huang, H. Zhang, *Chem. Soc. Rev.* **2015**, *44*, 2615.
[13] C. Hao, F. Wen, J. Xiang, S. Yuan, B. Yang, L. Li, W. Wang, Z. Zeng, L. Wang, Z. Liu, *Adv. Funct. Mater.* **2016**, *26*, 2016.
[14] D. Son, S. I. Chae, M. Kim, M. K. Choi, J. Yang, K. Park, V. S. Kale, J. H. Koo, C. Choi, M. Lee, *Adv. Mater.* **2016**, *28*, 9326.
[15] R. Ge, X. Wu, M. Kim, J. Shi, S. Sonde, L. Tao, Y. Zhang, J. C. Lee, D. Akinwande, *Nano Lett.* **2018**, *18*, 434.
[16] M.-Y. Li, S.-K. Su, H.-S. P. Wong, L.-J. Li, *Nature* **2019**, *567*, 169.
[17] Z. Shi, C. V. Singh, *Nanoscale* **2017**, *9*, 7055.
[18] J. Xiao, Z. Ye, Y. Wang, H. Zhu, Y. Wang, X. Zhang, *Light: Sci. Appl.* **2015**, *4*, e366.
[19] J. Yang, R. Xu, J. Pei, Y. W. Myint, F. Wang, Z. Wang, S. Zhang, Z. Yu, Y. Lu, *Light: Sci. Appl.* **2015**, *4*, e312.
[20] Y. Abate, S. Gamage, Z. Li, V. Babicheva, M. H. Javani, H. Wang, S. B. Cronin, M. I. Stockman, *Light: Sci. Appl.* **2016**, *5*, e16162.
[21] W. Strek, B. Cichy, L. Radosinski, P. Gluchowski, L. Marciniak, M. Lukaszewicz, D. Hreniak, *Light: Sci. Appl.* **2015**, *4*, e237.
[22] D. Wang, X.-B. Li, D. Han, W. Q. Tian, H.-B. Sun, *Nano Today* **2017**, *16*, 30.
[23] D. Wang, D. Han, X.-B. Li, S.-Y. Xie, N.-K. Chen, W. Q. Tian, S. Zhang, H.-B. Sun, *Appl. Phys. Lett.* **2016**, *109*, 203113.
[24] S. B. Zhang, *J. Phys.: Condens. Matter* **2002**, *14*, R881.
[25] S. H. Wei, *Comput. Mater. Sci.* **2004**, *30*, 337.
[26] C. Freysoldt, B. Grabowski, T. Hickel, J. Neugebauer, G. Kresse, A. Janotti, C. G. Van De Walle, *Rev. Mod. Phys.* **2014**, *86*, 253.
[27] Q. Cao, Y. W. Dai, J. Xu, L. Chen, H. Zhu, Q. Q. Sun, D. W. Zhang, *ACS Appl. Mater. Interfaces* **2017**, *9*, 18215.
[28] H. Fang, S. Chuang, T. C. Chang, K. Takei, T. Takahashi, A. Javey, *Nano Lett.* **2012**, *12*, 3788.
[29] S. Wi, H. Kim, M. Chen, H. Nam, L. J. Guo, E. Meyhofer, X. Liang, *ACS Nano* **2014**, *8*, 5270.
[30] A.-J. Cho, M.-K. Song, D.-W. Kang, J.-Y. Kwon, *ACS Appl. Mater. Interfaces* **2018**, *10*, 35972.
[31] T. Momose, A. Nakamura, M. Daniel, M. Shimomura, *AIP Adv.* **2018**, *8*, 025009.
[32] C. G. Van de Walle, P. Denteneer, Y. Bar-Yam, S. Pantelides, *Phys. Rev. B* **1989**, *39*, 10791.
[33] D. Wang, D. Han, X.-B. Li, S.-Y. Xie, N.-K. Chen, W.-Q. Tian, D. West, H.-B. Sun, S. B. Zhang, *Phys. Rev. Lett.* **2015**, *114*, 196801.
[34] T. Kanazawa, T. Amemiya, A. Ishikawa, V. Upadhyaya, K. Tsuruta, T. Tanaka, Y. Miyamoto, *Sci. Rep.* **2016**, *6*, 22277.
[35] M.-W. Lin, I. I. Kravchenko, J. Fowlkes, X. Li, A. A. Puretzky, C. M. Rouleau, D. B. Geohegan, K. Xiao, *Nanotechnology* **2016**, *27*, 165203.
[36] T. Pei, L. Bao, G. Wang, R. Ma, H. Yang, J. Li, C. Gu, S. Pantelides, S. Du, H.-J. Gao, *Appl. Phys. Lett.* **2016**, *108*, 053506.
[37] H. Liu, A. T. Neal, M. Si, Y. Du, D. Y. Peide, *IEEE Electron Device Lett.* **2014**, *35*, 795.
[38] N. R. Pradhan, D. Rhodes, S. Feng, Y. Xin, S. Memaran, B.-H. Moon, H. Terrones, M. Terrones, L. Balicas, *ACS Nano* **2014**, *8*, 5911.
[39] D. Wang, D. Han, X. B. Li, N. K. Chen, D. West, V. Meunier, S. Zhang, H. B. Sun, *Phys. Rev. B* **2017**, *96*, 155424.
[40] M. H. Naik, M. Jain, *Comput. Phys. Commun.* **2018**, *226*, 114.
[41] D. Vinichenko, M. G. Sensoy, C. M. Friend, E. Kaxiras, *Phys. Rev. B* **2017**, *95*, 235310.
[42] C. Freysoldt, J. Neugebauer, *Phys. Rev. B* **2018**, *97*, 205425.
[43] H.-P. Komsa, A. Pasquarello, *Phys. Rev. Lett.* **2013**, *110*, 095505.
[44] H.-P. Komsa, N. Berseneva, A. V. Krasheninnikov, R. M. Nieminen, *Phys. Rev. X* **2014**, *4*, 031044.
[45] T. J. Smart, F. Wu, M. Govoni, Y. Ping, *Phys. Rev. Mater.* **2018**, *2*, 124002.
[46] R. Sundararaman, Y. Ping, *J. Chem. Phys.* **2017**, *146*, 104109.
[47] F. Wu, A. Galatas, R. Sundararaman, D. Rocca, Y. Ping, *Phys. Rev. Mater.* **2017**, *1*, 071001.

[48] D. Han, D. West, X.-B. Li, S.-Y. Xie, H.-B. Sun, S. Zhang, *Phys. Rev. B* **2010**, *82*, 155132.
[49] S. Zhang, J. E. Northrup, *Phys. Rev. Lett.* **1991**, *67*, 2339.
[50] P. C. N. Pereira, S. W. S. Apolinario, *Phys. Rev. E* **2012**, *86*, 046702.
[51] J. Y. Noh, H. Kim, M. Park, Y. S. Kim, *Phys. Rev. B* **2015**, *92*, 115431.
[52] Y. Cui, R. Xin, Z. H. Yu, Y. M. Pan, Z. Y. Ong, X. X. Wei, J. Z. Wang, H. Y. Nan, Z. H. Ni, Y. Wu, T. S. Chen, Y. Shi, B. G. Wang, G. Zhang, Y. W. Zhang, X. R. Wang, *Adv. Mater.* **2015**, *27*, 5230.
[53] B. Radisavljevic, A. Radenovic, J. Brivio, V. Giacometti, A. Kis, *Nat. Nanotechnol.* **2011**, *6*, 147.
[54] J. P. Perdew, W. Yang, K. Burke, Z. H. Yang, E. K. U. Gross, M. Scheffler, G. E. Scuseria, T. M. Henderson, l. Y. Zhang, A. Ruzsinszky, H. W. Peng, J. W. Sun, E. Trushin, A. Gorling, *Proc. Natl. Acad. Sci. USA* **2017**, *114*, 2801.
[55] M. M. Ugeda, A. J. Bradley, S. F. Shi, F. H. da Jornada, Y. Zhang, D. Y. Qiu, W. Ruan, S. K. Mo, Z. Hussain, Z. X. Shen, F. Wang, S. G. Louie, M. F. Crommie, *Nat. Mater.* **2014**, *13*, 1091.
[56] M. H. Naik, M. Jain, *Phys. Rev. Mater.* **2018**, *2*, 084002.
[57] M. Chhowalla, D. Jena, H. Zhang, *Nat. Rev. Mater.* **2016**, *1*, 16052.
[58] J. Kang, W. Cao, X. Xie, D. Sarkar, W. Liu, K. Banerjee, in *Micro- and Nanotechnology Sensors, Systems, and Applications VI* (Eds: T. George, M. S. Islam, A. K. Dutta), SPIE, Bellingham, WA, **2014**. p. 7.
[59] F. Xia, H. Wang, Y. Jia, *Nat. Commun.* **2014**, *5*, 4458.
[60] Z. H. Yu, Z. Y. Ong, S. L. Li, J. B. Xu, G. Zhang, Y. W. Zhang, Y. Shi, X. R. Wang, *Adv. Funct. Mater.* **2017**, *27*, 1604093.
[61] J. Ahn, P. J. Jeon, S. R. A. Raza, A. Pezeshki, S.-W. Min, D. K. Hwang, S. Im, *2D Mater.* **2016**, *3*, 045011.
[62] S.-G. Yi, J. H. Kim, J. K. Min, M. J. Park, Y. W. Chang, K.-H. Yoo, *IEEE Trans. Nanotechnol.* **2016**, *15*, 499.
[63] D. Wang, D. Han, D. West, N.-K. Chen, S.-Y. Xie, W. Q. Tian, V. Meunier, S. Zhang, X.-B. Li, *npj Comput. Mater.* **2019**, *5*, 8.
[64] W. Zhou, X. Zou, S. Najmaei, Z. Liu, Y. Shi, J. Kong, J. Lou, P. M. Ajayan, B. I. Yakobson, J.-C. Idrobo, *Nano Lett.* **2013**, *13*, 2615.
[65] J. Hong, Z. Hu, M. Probert, K. Li, D. Lv, X. Yang, L. Gu, N. Mao, Q. Feng, L. Xie, *Nat. Commun.* **2015**, *6*, 6293.
[66] S. Das, W. Zhang, M. Demarteau, A. Hoffmann, M. Dubey, A. Roelofs, *Nano Lett.* **2014**, *14*, 5733.
[67] Y. Deng, Z. Luo, N. J. Conrad, H. Liu, Y. Gong, S. Najmaei, P. M. Ajayan, J. Lou, X. Xu, P. D. Ye, *ACS Nano* **2014**, *8*, 8292.
[68] H. Yuan, X. Liu, F. Afshinmanesh, W. Li, G. Xu, J. Sun, B. Lian, A. G. Curto, G. Ye, Y. Hikita, *Nat. Nanotechnol.* **2015**, *10*, 707.
[69] X. Cui, G.-H. Lee, Y. D. Kim, G. Arefe, P. Y. Huang, C.-H. Lee, D. A. Chenet, X. Zhang, L. Wang, F. Ye, *Nat. Nanotechnol.* **2015**, *10*, 534.
[70] D. A. Bandurin, A. V. Tyurnina, G. L. Yu, A. Mishchenko, V. Zólyomi, S. V. Morozov, R. K. Kumar, R. V. Gorbachev, Z. R. Kudrynskyi, S. Pezzini, Z. D. Kovalyuk, U. Zeitler, K. S. Novoselov, A. Patanè, L. Eaves, I. V. Grigorieva, V. I. Fal'ko, A. K. Geim, Y. Cao, *Nat. Nanotechnol.* **2017**, *12*, 223.
[71] L. Li, F. Yang, G. J. Ye, Z. Zhang, Z. Zhu, W. Lou, X. Zhou, L. Li, K. Watanabe, T. Taniguchi, *Nat. Nanotechnol.* **2016**, *11*, 593.
[72] V. Tayari, N. Hemsworth, I. Fakih, A. Favron, E. Gaufrès, G. Gervais, R. Martel, T. Szkopek, *Nat. Commun.* **2015**, *6*, 7702.
[73] L. Li, G. J. Ye, V. Tran, R. Fei, G. Chen, H. Wang, J. Wang, K. Watanabe, T. Taniguchi, L. Yang, *Nat. Nanotechnol.* **2015**, *10*, 608.
[74] D. Wang, X. B. Li, H. B. Sun, *Nanoscale* **2017**, *9*, 11619.
[75] J. Y. Noh, H. Kim, Y. S. Kim, *Phys. Rev. B* **2014**, *89*, 205417.
[76] S. Johnston, S. Kurtz, *J. Vac. Sci. Technol., A* **2006**, *24*, 1252.
[77] D. Wang, R. Sundararaman, *Phys. Rev. Mater.* **2019**, *3*, 083803.
[78] J. Ma, Z. G. Yu, Y. W. Zhang, *Phys. Rev. B* **2017**, *95*, 165447.
[79] H. Li, Z. Yin, Q. He, H. Li, X. Huang, G. Lu, D. W. H. Fam, A. I. Y. Tok, Q. Zhang, H. Zhang, *Small* **2012**, *8*, 63.
[80] M. R. Laskar, D. N. Nath, L. Ma, E. W. Lee, C. H. Lee, T. Kent, Z. Yang, R. Mishra, M. A. Roldan, J. C. Idrobo, S. T. Pantelides, S. J. Pennycook, R. C. Myers, Y. Wu, S. Rajan, *Appl. Phys. Lett.* **2014**, *104*, 092104.
[81] J. Suh, T.-E. Park, D.-Y. Lin, D. Fu, J. Park, H. J. Jung, Y. Chen, C. Ko, C. Jang, Y. Sun, R. Sinclair, J. Chang, S. Tongay, J. Wu, *Nano Lett.* **2014**, *14*, 6976.
[82] H. Li, G. Lu, Z. Yin, Q. He, H. Li, Q. Zhang, H. Zhang, *Small* **2012**, *8*, 682.